Integrin binding dynamics modulate ligand-specific mechanosensing in mammary gland fibroblasts

Martina Lerche[1], Alberto Elosegui-Artola[2], Camilo Guzmán[1], Maria Georgiadou[1], Jenny Z. Kechagia[2], Donald Gullberg[3], Pere Roca-Cusachs[2,4], Emilia Peuhu[1,5] ✉, and Johanna Ivaska[1,6] ✉

[1]Centre for Biotechnology, University of Turku and Åbo Akademi University, 20520 Turku, Finland
[2]Institute for Bioengineering of Catalonia, Barcelona 08028, Spain
[3]University of Bergen, Bergen, Norway
[4]University of Barcelona, Barcelona 08028, Spain
[5]FICAN West Cancer Research Laboratory, University of Turku and Turku University Hospital, 20520 Turku, Finland
[6]Department of Biochemistry, University of Turku, 20520 Turku, Finland

The link between the modulation of integrin activity and cellular mechanosensing of tissue rigidity, especially on different extracellular matrix ligands, remains poorly understood. Here, we find that primary mouse mammary gland stromal fibroblasts (MSFs) are mechanically distinct from previously studied cell types. In particular, MSFs generate high forces at a low matrix stiffness, equivalent to the soft mammary gland tissue, supported by maximal focal adhesion maturation, strong actin stress fiber formation, and myosin phosphorylation. We describe that loss of the cytosolic integrin inhibitor, SHARPIN, triggers impeded spreading of MSFs specifically on soft type I collagen but not on fibronectin. Through quantitative experiments and computational modelling, we find that reduced expression of the collagen-binding integrin α11β1 in SHARPIN-deficient MSFs leads to faster force-induced unbinding of adhesions from collagen. Faster unbinding, in turn, impairs force transmission in these cells, particularly, at the stiffness optimum observed for wild-type cells, and increases actin retrograde flow. Our results unveil a collagen-specific mechanosensing mechanism and suggest a key function for integrin activity regulation and integrin α11β1 in MSF mechanotransduction.

Integrin | Mechanotransduction | Focal adhesion | Collagen |Sharpin | Mammary gland | Magnetic tweezers | Traction force microscopy |

Correspondence: ***joivaska@utu.fi, emilia.peuhu@utu.fi***

Introduction

Fibroblasts exert high forces that are implicated in the morphogenetic rearrangement of extracellular matrices (ECMs) (1). In the developing mammary gland, stromal-cell-mediated organization of the ECM regulates mammary ductal morphogenesis (2, 3). Despite this important function, investigations into mammary stromal components are secondary to that of the mammary epithelium. In addition to ECM organization, mammary gland stromal fibroblasts (MSFs) also play a central role in the pro-invasive stiffening of breast tumor stroma (4), and therefore understanding the mechanical aspects of these cells is of clinical interest. While the role of integrins as cell mechanosensors and transducers is well established, the link between the regulation of integrin activity and the mechanosensing response on different ECM ligands remains poorly understood. SHARPIN is a cytosolic adaptor protein that, among other functions, binds to the intracellular integrin alpha tails and inhibits integrin activity *in vitro* and *in vivo* (5-8). We have previously demonstrated that stromal SHARPIN deficiency interferes with normal mouse mammary gland development and collagen fiber assembly *in vivo* (5). However, how and if SHARPIN mediates integrin-dependent mechanotransduction remains unresolved.

Collagen is abundant in the mammary gland stroma and plays a key role in regulating the physical and biochemical properties of the mammary gland. Alignment of stromal collagen bundles is critical for normal mammary gland development providing migration cues to the outgrowing duct during puberty (2, 3). The fibrillar collagen-binding integrin α11β1 has been linked to collagen remodeling and turnover (9, 10). In addition, in a mouse model of non-small cell lung cancer this integrin heterodimer induces cancer stromal stiffness (4). Furthermore, "trail blazer" breast cancer cells with high invasive capacity are characterized by high integrin α11β1 expression (11). Nevertheless, integrin α11β1 functions are rather poorly understood, and the role of this receptor in regulating cell-collagen interactions in the mammary gland has not been previously studied.

In order to sense the properties of the surrounding ECM, cells use dynamic molecular bonds, often referred to as molecular clutches, to exert forces within the cell boundary (12). A molecular clutch can be defined as a dynamic link between the ECM, integrin adhesion receptors, intracellular adaptor proteins, and the actomyosin cytoskeleton (13, 14). By quantification of the molecular clutch binding dynamics, and using mathematical modelling, one can predict the average force transmission of cells to the ECM as a function of substrate stiffness (13, 14).

Here, we have combined mathematical modelling with cell biology to investigate the biomechanical properties of primary mouse MSFs and to understand how the integrin activity regulator SHARPIN affects integrin-dependent force generation and mechanotransduction. We find that SHARPIN-deficient MSFs downregulate the collagen-binding integrin α11β1 resulting in a faster cell-collagen unbinding rate, and defective spreading specifically on collagen I -coated soft hydrogels with a stiffness corresponding to the

mammary gland tissue *in vivo*. Importantly, the molecular clutch model predicted that increased clutch unbinding rates, in SHARPIN-deficient cells on type I collagen, results in the loss of stiffness-dependent traction maximum and increased actin flow rates at low rigidities and these data were fully recapitulated experimentally in wild-type and SHARPIN-deficient primary MSFs. These data highlight an important divergence in the regulation of collagen I- and fibronectin-binding integrin heterodimers in the mammary gland stroma with implications for the mechanical response of fibroblasts. Moreover, these insights are likely to improve our understanding of fibrotic diseases including cancer where fibroblasts exhibit deregulated integrin activity (15, 16).

Results

Spreading of mouse mammary gland fibroblasts is differentially regulated on soft collagen I- and fibronectin-coated matrices. Based on previous observations that primary MSFs from SHARPIN-deficient (*Sharpin*$^{cpdm/cpdm}$; *Sharpin*^{cpdm}) mice have impaired capacity to contract collagen gels (5) we sought to investigate the link between integrin activity and force transduction. We first studied the ability of SHARPIN-expressing (*Sharpin*$^{+/+}$ or *Sharpin*$^{cpdm/+}$ from here on referred to as wild-type) and *Sharpin*^{cpdm} MSFs to spread in response to ECM stiffness and ligand type. MSFs were seeded on soft (2 kPa) fibronectin or collagen I precoated polyacrylamide gels, approximating the stiffness of the mammary tissue *in vivo* (5, 17, 18) (Fig. 1A). As expected based on the higher integrin β1 activity and faster focal adhesion (FA) turnover compared to wild-type MSFs (5, 7), *Sharpin*^{cpdm} MSFs appeared larger compared to wild-type MSFs when seeded on fibronectin-coated hydrogels (Fig. 1A, B). In contrast, on 2 kPa collagen I -coated hydrogels *Sharpin*^{cpdm} MSFs were less spread than wild-type MSFs (Fig. 1A, B). When cell size was measured on a stiffness range from 0.8-10 kPa (Fig. 1B), on collagen I-coated hydrogels, wild-type MSFs displayed a spreading optimum on 2 kPa, while *Sharpin*^{cpdm} MSFs appeared significantly smaller and only fully spread at 10 kPa (Fig. 1B). These data indicate that, at the stiffness range where MSFs are typically growing *in vivo*, SHARPIN supports MSF spreading specifically on collagen I, while the opposite is observed on fibronectin.

Given that *Sharpin*^{cpdm} MSFs have faster FA dynamics (increased assembly and disassembly rates) on collagen-coated rigid glass substrate (5), we next evaluated the effect of SHARPIN deficiency on FA maturation (number and average length) on a range of hydrogel rigidities. Vinculin, a mechanosensitive adaptor molecule recruited to mature FA (19, 20), was immunolabeled in wild-type and *Sharpin*^{cpdm} MSFs plated on 0.8-10 kPa collagen I-coated hydrogels (Fig. 1C). While quantitative image analysis of vinculin-containing adhesions at the cell edges in wild-type and *Sharpin*^{cpdm} MSFs (Fig. S1A) demonstrated a similar number of FA per cell on collagen I -coated hydrogels (Fig. 1D), the maximum elongation of FA occurred on slightly higher stiffness in *Sharpin*^{cpdm} MSFs (Fig. 1E). In contrast, on fibronectin, *Sharpin*^{cpdm} MSFs demonstrated an increased number of edge FA on 4 kPa hydrogels (Fig. S1B) and slightly enhanced elongation of FA at 2 kPa (Fig. S1C), consistent with the increased cell spreading (Fig. 1A, B). Unexpectedly, neither genotype displayed the typical reinforcement of adhesion maturation with increasing stiffness, usually mirrored by an increase in length of vinculin adhesions (13). Instead, both wild type and *Sharpin*^{cpdm} primary MSFs formed mature, vinculin-containing adhesions on soft collagen I -coated matrices reaching the maturation maxima already on 2-4 kPa (Fig 1E), and also exhibited nuclear localization of the mechanosensitive transcription factor Yes-associated protein 1 (YAP1) at this low stiffness (Fig. S1D, E). This localization was reduced in *Sharpin*^{cpdm} MSFs (Fig. S1D, E) The ability of MSFs to generate growing adhesions with connections to the actin cytoskeleton on a low stiffness is exceptional, when compared to another fibroblast type (13), and may be linked to the soft mammary gland environment from which these primary cells were isolated (5, 17, 18). In conclusion, *Sharpin*^{cpdm} MSFs demonstrate reduced capacity to spread on soft collagen I-coated matrices, while the opposite occurs on fibronectin-coated substratum.

Integrin α11β1 protein levels regulate the spreading of MSFs on soft matrices. In order to explain the observed ligand-specific phenotypes in MSFs (Fig 1A-B), we next sought to investigate whether the wild-type and *Sharpin*^{cpdm} MSFs would display differences in integrin expression levels. An RNA sequencing dataset of wild-type and *Sharpin*^{cpdm} MSFs (5) was analyzed for all the matrix-binding integrin subtypes (Fig. S2A). Of the collagen-binding integrin alpha subunits (*Itga1, Itga2, Itga10, Itga11*), which all form a heterodimer with the integrin β1 subunit, *Itga11* was the predominant α-subunit expressed at mRNA level, *Itga1* was detected at low levels and *Itga10* or *Itga2* were not detected. Of the fibronectin-binding integrins, *Itga5* and *Itgav*, which both pair with integrin β1, were the most highly expressed. In addition, MSFs expressed low levels of *Itgb3* and high levels of *Itgb5*, both of which form a heterodimer with integrin αv. Importantly, no significant differences in integrin mRNA expression levels were observed between wild-type and *Sharpin*^{cpdm} (Fig. S2A).

Next, we analyzed the cell-surface densities of both total and active integrin β1 with conformation-specific antibodies. *Sharpin*^{cpdm} MSFs displayed lower levels of total integrin β1, but similar levels of the active integrin β1 conformation (antibody clone 9EG7) on the cell-surface compared to wild-type cells (Fig. 2A). Thus, a higher proportion of cell-surface integrins appear to be in an active state in the absence of SHARPIN (Fig. 2B), in line with our previous studies with MSFs (5) and other cell types (6, 7). Then, we analyzed the cell-surface protein levels of integrin β1-binding α-subunits and found that *Sharpin*^{cpdm} MSFs had slightly downregulated levels of integrin α5, but significantly reduced levels of integrins α1 and α11 on the cell surface compared to wild-type MSFs (Fig. 2C). Analysis of the total protein levels of integrin α11 by western blotting confirmed the lower expression of integrin α11 in *Sharpin*^{cpdm} MSFs (Fig. 2D, E; mouse integrin α1 protein levels were not analyzed with western blot-

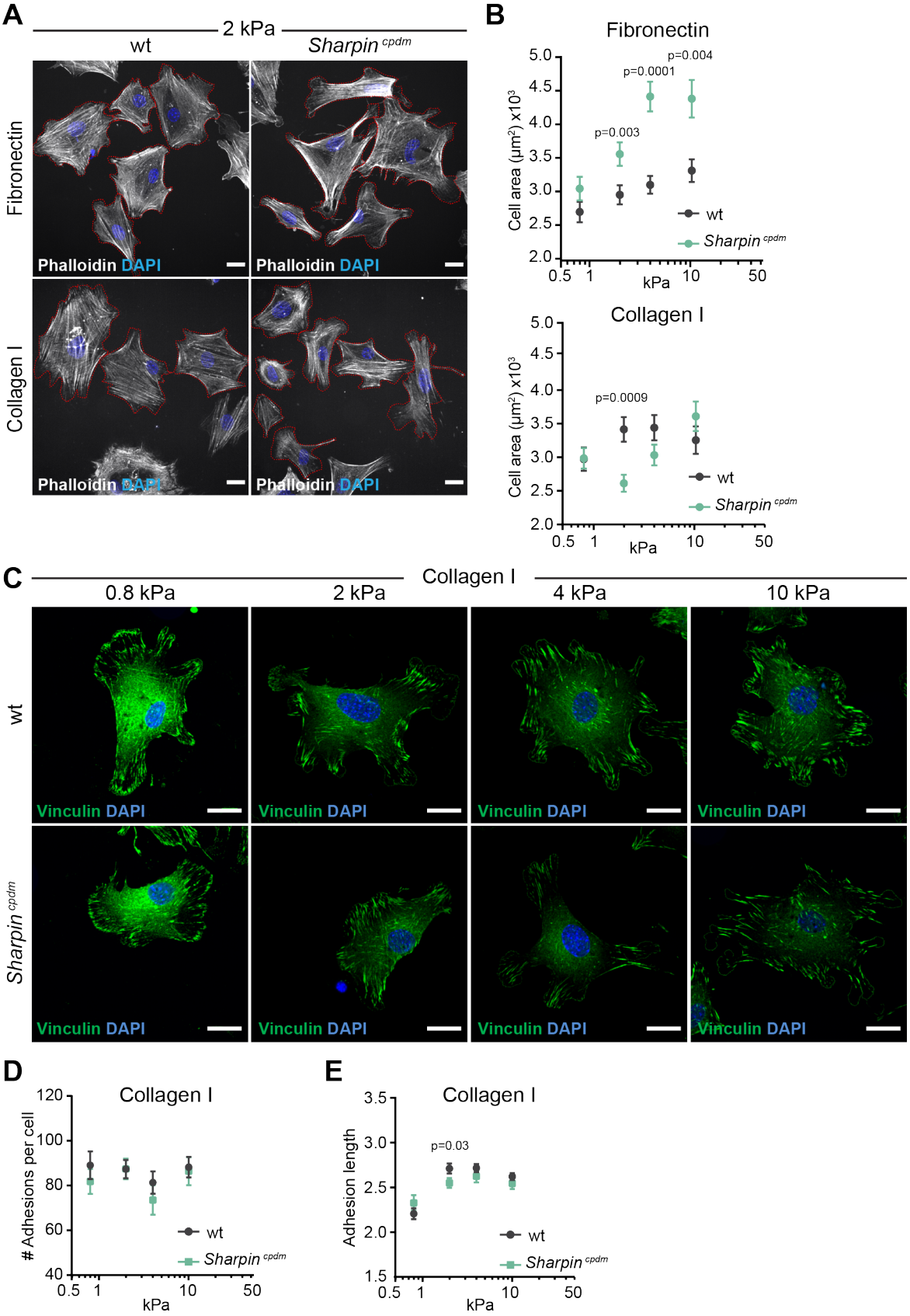

Fig. 1. Spreading of mouse mammary gland fibroblasts (MSFs) is regulated differentially on soft collagen- and fibronectin-coated matrices. A) Representative images of wild-type and *Sharpin*^{cpdm} MSFs plated for 3-4h on 2 kPa fibronectin (upper panel) or collagen I (lower panel)-coated polyacrylamide (PAA) hydrogels and labelled for F-actin (white) and nuclei (blue). Cell edges are outlined with red dashed line. **B)** Quantification of cell spreading on 0.8-10 kPa PAAs coated with fibronectin (upper panel) or collagen I (lower panel) based on immunofluorescence. Data are pooled from 3 independent experiments, n=72-103 cells (fibronectin) and n=59-118 cells (collagen I). **C)** Representative images of vinculin-containing FAs (green) in wild-type and *Sharpin*^{cpdm} MSFs plated for 3-4 h on 0.8-10 kP collagen I-coated PAA hydrogels, nuclei (blue) were co-labelled. Quantification of the number of FA per cell **D)** and the length of FA **E)** in MSFs plated on collagen I-coated 0.8-10 kPa PAA hydrogels. Data are pooled from three independent experiments, n=41-109. Mean ± SEM in all graphs. Mann–Whitney test. Scale bars represent 20 µm.

ting due to the lack of suitable antibodies), and the lower expression levels were also observed by immunofluorescence labeling of integrin α11 in cells plated on collagen I-coated 2 kPa hydrogels (Fig. 2F). Furthermore, a reduced protein level of integrin α11 was observed also in *Sharpin*^{cpdm} MSFs that were seeded on 2 kPa collagen I-coated hydrogels directly after isolation from the mouse mammary gland (Fig. S2B), indicating that the observed difference in integrin α11 is not induced by *in vitro* culture on stiff substratum (plastic). Together, these data show that SHARPIN-deficiency leads to reduced cell surface expression of collagen-binding integrin heterodimers in MSFs, and causes reduced expression of integrin α11 at the protein level, but does not affect the transcription of integrins.

To investigate whether the strongly reduced surface expression of integrin α1 and α11 in *Sharpin*^{cpdm} MSFs could be responsible for the impaired capability to spread on a compliant collagen I-coated surface, we analyzed cell spreading following siRNA-mediated downregulation of integrin α1 or integrin α11 (Fig. 2G), confirmed by qPCR (Fig. S2C). In wild-type MSFs downregulation of integrin α11, but not integrin α1, led to significantly reduced cell spreading on 2 kPa collagen I-coated hydrogels that resembled the phenotype of *Sharpin*^{cpdm} MSFs (Fig. 2G). In contrast, no significant differences in cell area were seen in *Sharpin*^{cpdm} MSFs (with endogenously lower integrinα1 and integrin α11 levels; Fig 2C) after downregulation of integrin α1 or integrin α11 (Fig. 2G). These data indicate that appropriate levels of integrin α11, but not integrin α1, are important for regulating the spreading of MSFs on soft collagen I-coated substrates. Interestingly, previous data has demonstrated that the integrin α1I domain has a low binding affinity to fibrillar collagens (types I, II and III) compared to the integrin α2I domain (21). Since α1 and α11 are the main collagen-binding integrins expressed in MSFs (Fig. S2A), it is possible that integrin α11 acts as the major type I collagen binding integrin in these cells. However, this remains to be investigated.

To further test whether SHARPIN regulates integrin α11 protein expression, we silenced SHARPIN using a previously well-validated siRNA oligo (5) in wild-type MSFs (Fig. 2H, I). Indeed, siRNA-mediated downregulation of SHARPIN led to reduced integrin α11 protein levels compared to control silencing (Fig. 2H, I). To verify that integrin α11 promotes cell spreading on soft substratum, we ectopically expressed EGFP-tagged human integrin α11 in MSFs, allowed the cells to spread for 4 h on collagen I-coated 2 kPa hydrogels and quantitatively analyzed the cell area (Fig. 2J, K). Reintroduction of integrin α11 reversed the defective cell spreading of *Sharpin*^{cpdm} MSFs on collagen I, whereas cell area in wild-type MSFs was not significantly affected (modest decrease) by the overexpression of integrin α11-EGFP (Fig. 2J, K). In conclusion, these data demonstrate that integrin α11β1 is essential in spreading of MSFs on soft collagen I-coated substrates and that SHARPIN promotes cell spreading by regulating integrin α11β1 protein expression level.

Integrin α11β1 plays a key role in MSF integrin-collagen binding dynamics. We then assessed how the altered integrin activity and expression level in *Sharpin*^{cpdm} MSFs affects cell-ECM mechanical interactions, by evaluating in detail the binding and unbinding properties of the cells to matrix ligands (Fig. 3A). First, we analyzed, by immunofluorescence, the recruitment of integrin β1 to silica beads coated with collagen I or fibronectin. *Sharpin*^{cpdm} MSFs displayed slightly increased recruitment of integrin β1 to collagen I when compared to wild-type cells, while no significant differences in binding to fibronectin-coated beads were observed (Fig. 3B). We then employed a magnetic tweezers setup (14), a method that allows quantitative measurement of the strength of receptor-ligand bonds, to apply force to collagen I or fibronectin-coated beads attached to cells, and evaluated the time required to detach beads from cells (Fig. 3C). Detachment times of collagen-coated beads were greatly decreased for *Sharpin*^{cpdm} MSFs (Fig. 3C). In line with the bead recruitment experiments (Fig. 3B), no significant differences were observed in integrin detachment time when using fibronectin as an ECM ligand (Fig. 3C). These data demonstrate a striking increase in integrin-collagen I binding dynamics in SHARPIN-deficient cells.

As SHARPIN was found to influence integrin α11 protein levels and subsequently cell spreading in MSFs (Fig. 2), we hypothesized that the observed increase in collagen I unbinding rate would be due to a reduced amount of integrin α11 clutches in *Sharpin*^{cpdm} MSFs. To investigate this, we measured the relative detachment time of collagen I-coated magnetic beads in *Sharpin*^{cpdm} MSFs that overexpressed integrin α11-EGFP. Interestingly, the reintroduction of integrin α11 by ectopic expression partially rescued the ligand detachment time in *Sharpin*^{cpdm} MSFs (Fig. 3D). Taken together, these results indicate that lack of SHARPIN impairs the integrin-collagen I binding dynamics of MSFs largely via integrin α11 downregulation.

Molecular clutch model predicts the absence of traction peak in *Sharpin*^{cpdm} cells at biologically relevant rigidities. We next studied the phosphorylation of myosin light chain 2 (pMLC2) as a measure for actomyosin contractility, which is an important component of the molecular clutch. In contrast to mouse embryonic fibroblasts (MEFs) where pMLC2 levels appeared to be independent of substrate stiffness (Fig. S3A) (13), pMLC2 levels were increased in MSFs in response to increasing stiffness (Fig. 4A, Fig. S3A, B) similar to other previously described cells (22). Furthermore, higher pMLC was observed in MSFs plated on soft substrate as compared to MEFs (Fig. S3A). However, no significant differences in pMLC2 were detected between wild-type and *Sharpin*^{cpdm} MSFs, suggesting that myosin contractility remains predominantly unaffected in the absence of SHARPIN. In all, these results support the hypothesis that SHARPIN regulates cell mechanosensing by modulating the activity and expression level of collagen binding integrins. Our data suggest that the threshold for talin unfolding and FA reinforcement through cytoskeletal interaction and contractility (13) would occur in MSFs on very soft rigidities, highlighting the unique mechanistic properties of primary MSFs.

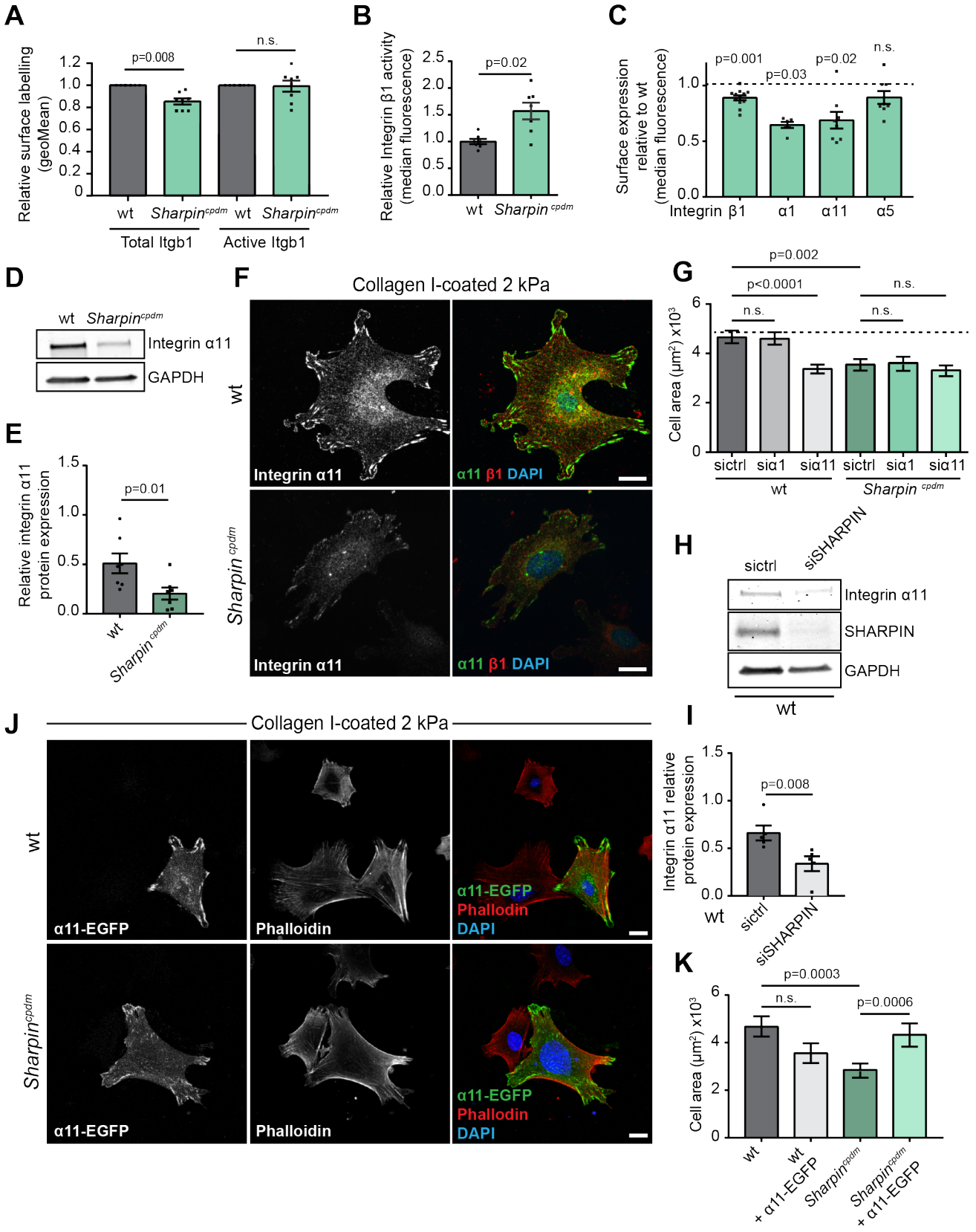

Fig. 2. Integrin α11β1 protein levels regulate the spreading of MSFs on soft matrices. A) Quantification of total (clone: HMβ1-1) and active (clone: 9EG7) integrin β1 cell surface levels (n=8) **A)** and relative integrin β1 activity (n=7) **B)** in *Sharpin*^{cpdm} and wild-type MSFs, and measurement of cell surface expression of integrin β1 binding α-subunits in *Sharpin*^{cpdm} relative to wild-type MSFs (n = 6-12) **C)**. Surface expression levels in flow cytometry relative to wild-type MSFs are shown. **D)** Representative Western blot analysis of integrin α11 protein expression in wild-type and *Sharpin*^{cpdm} MSFs, and **E)** quantification of the relative integrin α11 expression levels (n=7). GAPDH was detected for loading control. **F)** Representative images of immunolabelled integrin α11 (green) and active integrin β1 (red) in wild-type and *Sharpin*^{cpdm} MSFs plated on 2 kPa collagen I-coated PAA hydrogels. Nuclei (blue) were co-labelled. Scale bar represents 20 μm. **G)** Quantification of the cell area in wild-type and *Sharpin*^{cpdm} MSFs silenced with control, integrin α1 and integrin α11 targeting siRNA and plated on 2 kPa collagen I-coated PAA hydrogels; n=82-94 cells from three independent experiments. Mean ± SEM. **H)** Representative Western blot analysis of integrin α11 and SHARPIN protein expression in wild-type MSFs silenced with control and SHARPIN-targeting siRNA, and **I)** quantification of the relative integrin α11 expression levels (n=5). GAPDH was detected for loading control. **J)** Representative images of integrin α11-EGFP transfected wild-type and *Sharpin*^{cpdm} MSFs plated on 2 kPa collagen I-coated PAA hydrogels, and co-labelled for F-actin (red) and nuclei (blue). **K)** Quantification of cell area in non-transfected and integrin α11-EGFP transfected wild-type and *Sharpin*^{cpdm} MSFs plated on 2 kPa collagen I-coated PAA hydrogels. Data are pooled from two independent experiments (n=41-57 cells). Scale bars represent 20 μm. **B,E,I,K)** Mann-Whitney test, **A,C)** Wilcoxon matched-pairs signed rank test. **G)** unpaired t-test.

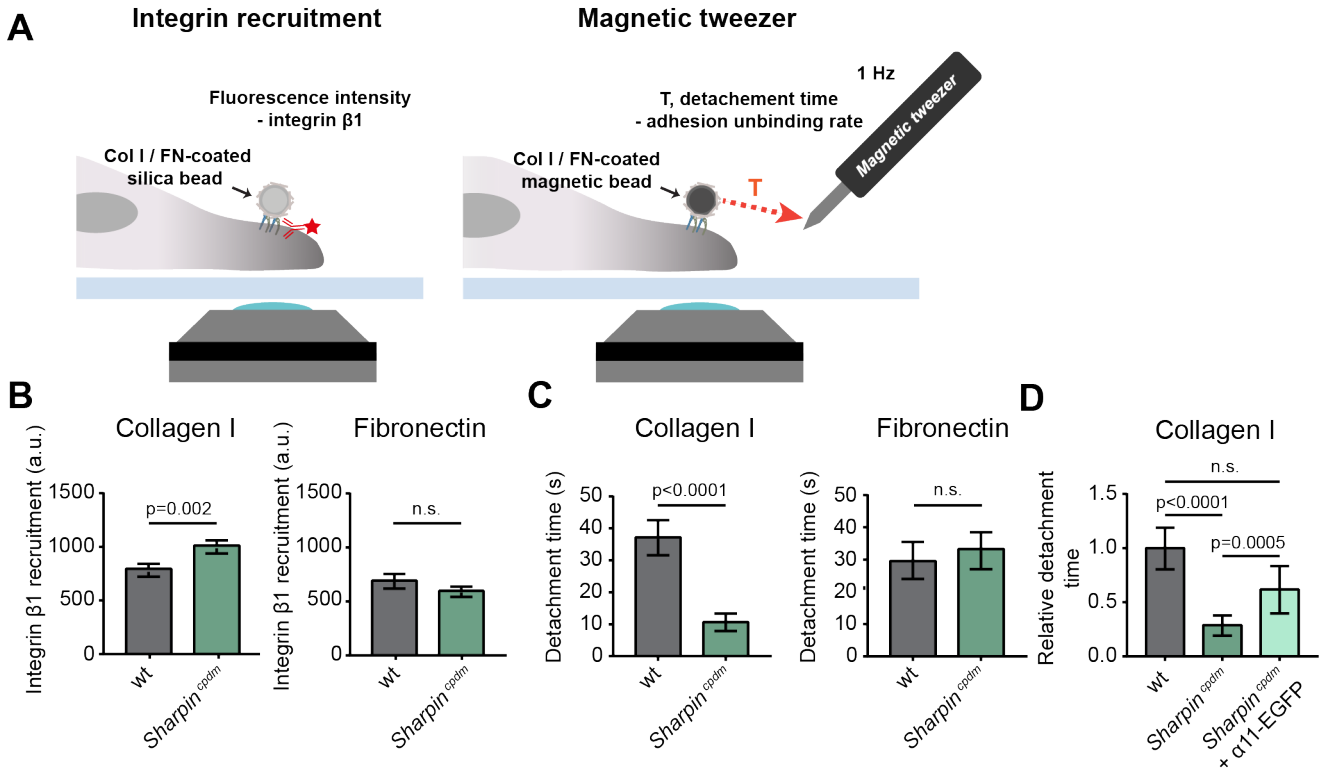

Fig. 3. Integrin α11β1 plays a key role in integrin-collagen binding dynamics of MSFs. A) Schematic representation of the set up for integrin recruitment (left) and magnetic tweezer (right) experiments. **B)** Quantification of Itgb1 recruitment to collagen I (left panel) or fibronectin (right panel) -coated silica beads; n=51-62 (collagen I) and 33-34 (fibronectin) from 2 independent experiments. **C)** Quantification of the detachment time of wild-type and *Sharpin*^{cpdm} MSFs from collagen I (left panel) or fibronectin (right panel) -coated magnetic beads; n=34 (collagen) and 29-37 (fibronectin) from 2 independent experiments. Mean ± SEM in all graphs. **D)** Quantification of the detachment time of wild-type, *Sharpin*^{cpdm}, integrin α11 -EGFP transfected *Sharpin*^{cpdm} MSFs from collagen I-coated magnetic beads. Data are pooled from three independent experiments (n=46-101). Mean ± SEM in all graphs. **B,C)** unpaired t-test, **D)** Mann-Whitney test. Col I, collagen I; FN, fibronectin.

In mechanical terms, the main effect induced by SHARPIN deficiency was a very strong reduction in the ability of integrin-collagen I adhesions to withstand force, as assessed by magnetic tweezers experiments (Fig. 3C, D). Because the binding of β1 integrins to collagen I-coated beads was not strongly affected (and in fact slightly increased, Fig. 3B) by SHARPIN-deficiency, reduction in adhesion strength could not be explained by a defect in integrin recruitment (i.e., reduction in the number of integrin clutches). Instead, the reduced spreading of *Sharpin*^{cpdm} MSFs on collagen (Fig. 1A, B) was consistent with an increase in the unbinding rates of integrin-collagen I bonds under force (Fig. 3C). According to the molecular clutch model of adhesion (14, 23), if myosin contractility levels are not affected, such an increase in unbinding rate should strongly affect cell mechanosensing, via traction force generation.

To test this, we measured cell-matrix force transmission using traction force microscopy. In wild-type cells on collagen I, and as predicted by the molecular clutch model (Fig. 4B), we observed a biphasic response of force as a function of stiffness, with a force maximum at 2 kPa (Fig. 4C). We note that this biphasic response (Fig. 4B) is the prediction obtained when only clutch dynamics are considered, without introducing changes in integrin recruitment or adhesion growth as a function of stiffness (13, 14). We also note that such changes would not be applicable here, since MSFs displayed mature adhesions at all rigidities tested (Fig 1C, E). If integrin unbinding rates are increased, as observed in *Sharpin*^{cpdm} cells, the model prediction is that the link between actin and the substrate is weakened, thus reducing the forces and the intensity of the force peak, and increasing actin flow.

As predicted (Fig. 4B), *Sharpin*^{cpdm} cells do not exhibit a force maximum at 2 kPa collagen I-coated hydrogels (Fig. 4C). Accordingly, the respective trends in wild-type and *Sharpin*^{cpdm} cells could be reproduced by the molecular clutch model simulations in which we only altered integrin unbinding rates between conditions. Consistent with the fact that no differences in adhesion behavior under force were observed with fibronectin-coated beads (Fig. 3C), wild-type and *Sharpin*^{cpdm} cells exerted the same forces on fibronectin-coated substrates irrespective of stiffness (Fig. 4D). Additionally, as predicted, actin flows of actively spreading (plated for less than 30 minutes) *Sharpin*^{cpdm} cells (average 51 nm/s) on 2 kPa collagen I-coated hydrogels were increased with respect to wild-type cells (average 35 nm/s) (Fig. 4E, F). Interestingly, in stably adhered MSFs (plated for 4 hours) on 2 kPa collagen I-coated hydrogels, very slow actin retrograde flow was observed compared to MEFs (Fig. S3C), and measurement of actin flows in MSFs was beyond the detection limit. This is a stark contrast to the rapid actin flow detected in cells derived from other tissues on soft substrate (13, 24, 25), further demonstrating that the MSFs have distinct mechanistic properties reflecting their natural soft *in vivo* environment.

Interestingly, when MSFs were allowed to spread on collagen I-coated crossbow-shaped micropatterns on top of 2 kPa hydrogels thereby standardizing the cell-shape and polarity, a larger fraction of wild-type MSFs displayed an aligned orientation of actin fibers (perpendicular to cell axis) com-

pared to *Sharpin*^{cpdm} MSFs (Fig. 4G, H). This suggests that the increased integrin-collagen unbinding (Fig. 3C) and reduced capacity to produce traction forces on soft collagen-coated substratum (Fig. 4C) due to SHARPIN deficiency also translate into defects in actin cytoskeletal organization in a biologically relevant substrate stiffness, which is an important aspect in cell polarization.

Together, these data demonstrate that SHARPIN deficiency, and the consequent increase in integrin-collagen unbinding rate, leads to significant effects in mechanotransduction in MSFs, providing a possible explanation to our previous finding that *Sharpin*^{cpdm} MSFs are unable to remodel collagen *in vitro* and are defective in supporting generation of mammary gland stromal architecture supportive of normal development and ductal outgrowth (5).

Discussion

The differential regulation of collagen- and fibronectin-binding integrins, and the mechanobiological implications of these differences remain poorly understood. Here, we have investigated the consequences of SHARPIN-deficiency on cell mechanosensing, integrin ligand-binding dynamics, and traction force generation, and conducted mathematical modelling of these events. Our data using primary mouse MSFs demonstrate that in the absence of the integrin activity regulator SHARPIN, the expression of the collagen-binding integrin α11β1 is downregulated, which leads to defective ability of MSFs to spread and create traction forces specifically on collagen-coated soft hydrogels. Importantly, the molecular clutch model was able to predict the absence of traction peak and increased actin flow rate at low rigidities based on increased clutch unbinding rates measured by magnetic tweezers in SHARPIN-deficient cells. Although SHARPIN regulates the activity of both collagen and fibronectin -binding integrins (7), these data demonstrate that their expression levels undergo differential regulation upon increased integrin activity. Consequently, different influences on the mechanosensitive response are observed on collagen and fibronectin in SHARPIN-deficient MSFs.

Since its relatively late discovery (26), integrin α11β1 has been linked to the regulation of collagen contractility (9, 10) and to fibroblast-associated disease conditions, such as fibrosis and cancer (4, 27). Integrin α11β1 is expressed in various types of fibroblasts including cancer-associated fibroblasts (28) as well as in invasive cancer cells (11) and mesenchymal stem cells (29). We did not observe changes in integrin α11 expression at the transcriptional level in *Sharpin*^{cpdm} fibroblasts. However, at the protein level integrin α11 was strongly downregulated in SHARPIN-deficient MSFs and in wild-type MSFs upon SHARPIN silencing, indicating that SHARPIN is required for integrin α11 stability via a yet undefined mechanism.

The regulatory pathways modulating the activity of collagen-binding integrins may be distinct from other integrin heterodimers. The vast majority of studies investigating integrin activation are based on the platelet-specific integrin αIIbβ3 and the fibronectin receptors integrin α5β1 and αvβ3, which are primarily regulated by inside-out and outside-in signaling. In turn, only a few studies have addressed activity regulation in the context of collagen-binding integrins. Heterodimerization of α1β1 and α2β1 integrins has been postulated to have a key role in their activity regulation based on the lower affinity of integrin α1 and α2 to integrin β1 (30). Thus, regulation of the expression levels of collagen-binding integrins may be particularly important for their ligand binding dynamics. The fact that in *Sharpin*^{cpdm} cells, collagen-coated beads demonstrated increased integrin β1 recruitment, but decreased resistance of the integrin-collagen links to force, suggests that integrin α11β1 competes for collagen binding with other integrin β1 heterodimers, namely α1β1 in MSFs, and that different integrin-collagen bonds have different force responses. However, this hypothesis remains to be investigated.

Our results provide a striking example of how, even if major mechanical regulators such as myosin contractility are not affected, merely changing integrin properties under force can dramatically affect the cell's mechanoresponse. Interestingly, the fact that wild-type MSFs exhibit mature, vinculin-associated FA irrespective of matrix stiffness allowed us to decouple traction force generation from adhesion maturation, leading to the fundamental clutch model prediction of a biphasic traction-stiffness relationship that is otherwise very elusive to observe (12). We also note that both wild-type and SHARPIN-deficient cells exhibit a final increase in force transmission with stiffness that is not predicted by the model. Whereas the nature of this regime remains unknown and warrants further investigation, we note that in conditions with very small actin flows and very stable adhesions and actin fibers, cytoskeletal reorganization events other than fast actin flows could be determinant of the cellular force transmission (31).

Together, our findings demonstrate how altered integrin activity in SHARPIN-deficient primary MSFs results in deregulated cell spreading and traction force generation in response to substrate ligand composition and stiffness. The concurrently observed defects in actin cytoskeletal organization and nuclear translocation of the mechanosensitive transcription factor YAP in *Sharpin*^{cpdm} MSFs could also be linked to the inability of these cells to support normal stromal composition and mammary gland development (5). The central role for integrin α11, uncovered here, in regulating mechanotransduction on collagen may also be essential to the pathological behavior of fibroblasts in cancerous or fibrotic tissues. As both SHARPIN and integrin α11β1 are significant regulators of cancer tumorigenesis and dissemination, as well as fibroblast contractility and collagen remodeling (4, 5, 32-34), increased understanding of their functional interplay is of wide interest. Finally, our finding that the mechanical output of fibroblasts can be strongly influenced by a single parameter of the molecular clutch, the integrin binding dynamics, highlights the tuneability of mechanotransduction, and its ability to trigger specific outputs in response to both internal and external parameters.

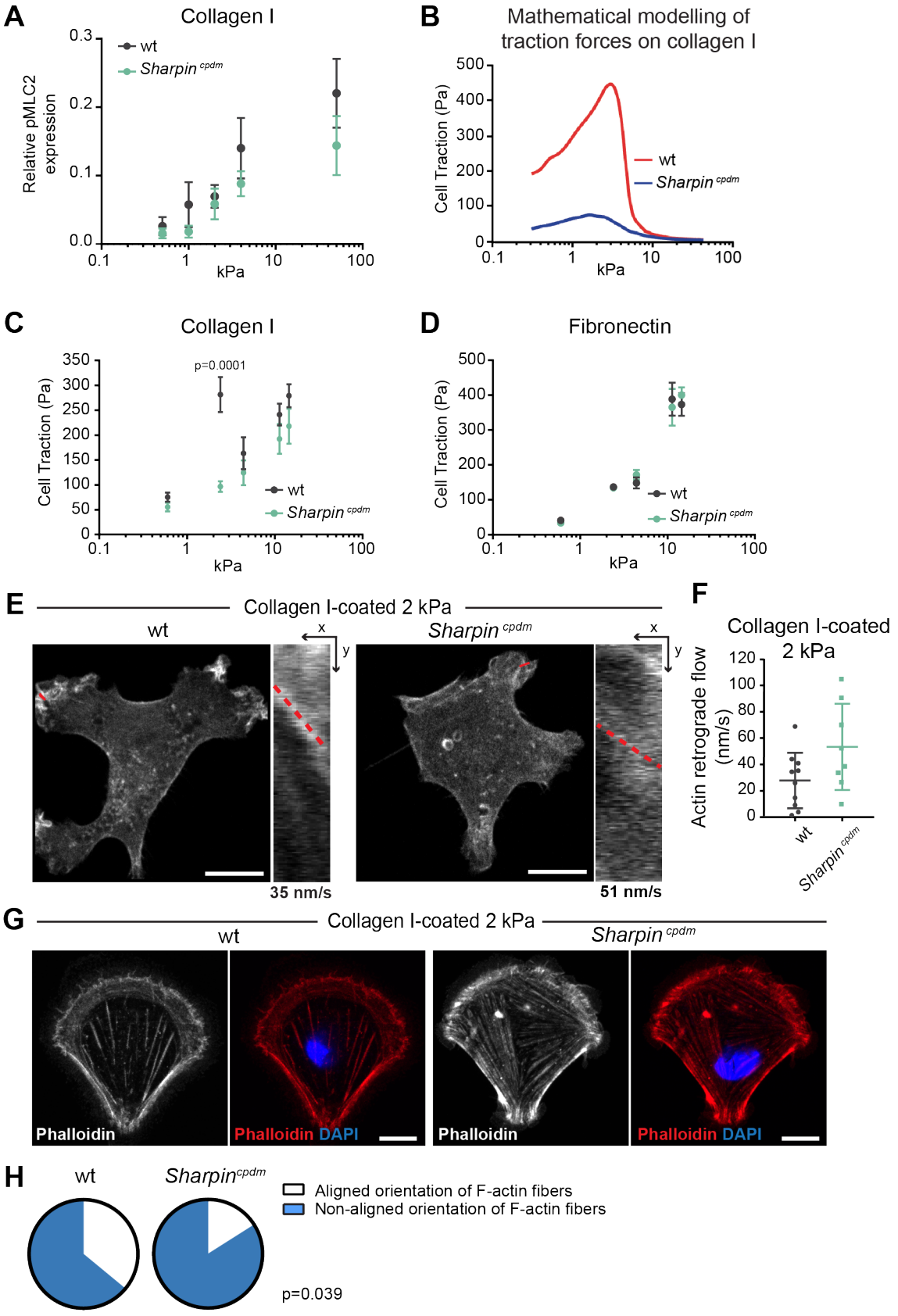

Fig. 4. Molecular clutch model predicts the absence of traction peak in SHARPIN-deficient cells at biologically relevant rigidities. A) Quantification of relative pMLC2 expression levels in wild-type and *Sharpin*^{cpdm} MSFs plated on collagen I-coated PAA hydrogels of indicated stiffness (n= 3). **B)** Prediction of the traction forces generated by wild-type and *Sharpin*^{cpdm} MSFs on collagen I-coated PAA hydrogels based on molecular clutch model. **C)** Average forces exerted by wild-type and *Sharpin*^{cpdm} MSFs on collagen I-coated PAA hydrogels of indicated stiffness measured by traction force microscopy (n=17-25 cells from 2 independent experiments. **D)** Average forces exerted by wild-type and *Sharpin*^{cpdm} MSFs on fibronectin-coated PAA hydrogels of indicated stiffness measured by traction force microscopy (n=10-23 cells from 2 independent experiments) Mean ± SEM in all graphs. **E)** Representative images of LifeAct-GFP transfected wild-type and *Sharpin*^{cpdm} MSFs plated on 2 kPa collagen I-coated PAA hydrogels. Insets are kymographs showing actin retrograde flow along the red line (time=180s, imaged every second). The slope of the line was used to calculate the actin retrograde flow rate. **F)** Quantification of actin retrograde flow; data pooled from 3 independent experiments, n=8-10. **G)** Representative images of wild-type and *Sharpin*^{cpdm} MSFs plated on collagen I-coated crossbow micropatterns on 2 kPa PAA hydrogels, and labelled for F-actin (red) and nuclei (blue). Scale bars represent 10 µm **H)** Quantification of cells with aligned orientation and non-aligned orientation of actin ventral stress fibers n=50 cells from 3 independent experiments. Mean ± SEM in all graphs. **A)** Mann–Whitney U-test,**H)** Fisher's exact test (p=0.039).

Materials and methods

Animals. The C57BL/KaLawRij-*Sharpin*^{cpdm}/RijSunJ mouse strain (Stock No: 007599) with a spontaneous mutation leading to the complete loss of SHARPIN protein (35, 36) was acquired from The Jackson Laboratory (Bar Harbor, ME). The colony was maintained and genotyped as previously described (5). Six to seven week-old, female *Sharpin*^{cpdm}(*Sharpin*$^{cpdm/cpdm}$) mice and littermate wild-type mice (*Sharpin*$^{+/+}$ or *Sharpin*$^{+/cpdm}$) were used for MSFs isolation. Mice were housed in standard conditions (12-h light/dark cycle) with food and water available *ad libitum*. The viability, clinical signs and behaviour of the mice were monitored daily. For euthanasia, cervical dislocation was used in conjunction with CO2. All animal experiments were ethically assessed and authorised by the National Animal Experiment Board and in accordance with The Finnish Act on Animal Experimentation (Animal licence number ESAVI-9339-04.10.07-2016).

Isolation of primary cells. Isolation of MSFs was performed as previously described (5). Briefly, mouse mammary glands were dissected after sacrifice, lymph nodes removed and the tissue moved to ice cold PBS. The tissue was first mechanically disrupted by mincing with scalpel followed by 2-3 h enzymatic digestion (1% L-glutamine, insulin 5 µg/ml, gentamycin 50 µg/ml, 5% FCS and 2 mg/ml collagenase in DMEM/F-12), and DNAse I treatment (20 U/ml). Fibroblasts were isolated by repeated pulse centrifugation (1500 rpm) and collecting each time the supernatant that contained the stromal cells. After the last pulse centrifugation, the collected supernatant was pelleted and resuspended in growth medium (1% L-glutamine, 1% penicillin/streptomycin, 5% FCS in DMEM/F-12) and the cells plated for culture. Medium was replaced the next day to remove non-adherent and dead cells.

Transient transfection and gene silencing. Plasmids [mEmerald-Lifeact-7 (addgene, #54148) and hITGA11-GFP (pBJ1 human integrin alpha 11-EGFP; Erusappan, P., et al. Integrin α11 cytoplasmic tail is required for FAK activation to initiate 3D cell invasion and ERK-mediated cell proliferation. Manuscript in preparation)] were transfected using DNA-In reagent (GST-2131, MTI Global Stem) or Lipofectamine 3000 (L3000075, ThermoFisher according to the manufacturer's instructions. Briefly a transfection mixture of DNA-In reagent and plasmid was prepared in 1:3 ratio (µg DNA: µl DNA:In) in 250 µl optimum and incubated for 15 min before transfection. The transfection mixture was added to adhered cells grown on a 6-well plate in 2.5 ml fresh media and cells incubated for 24 h. For transfection with Lipofectamine 3000 reagent a mixture of ratio 4:4:2.5 (µl Lipofectamine 3000 reagent: µl P3000TM Enhancer reagent: µg DNA) was prepared in 500 µl optimem and incubated for 15 minutes before adding to adhered cells grown on a 6-well plate in 2 ml fresh antibiotic free media and cells incubated for 24 h. ON-TARGETplus Mouse Itga1 (109700; 5'-CUU UAA UGA CGU CGU GAU U-3', 5´-GCC UAU GAC UGG AAC GGA A-3', 5´-CCA CAA UUG ACA UCG ACA A-3', and5'-AGG GCA AGG UGU ACG UGU A-3') and Mouse Itga11 (319480; 5'-AUG GAU GAG AGG CGG UAU A-3´, 5'-UCA GAA GAC AGG AGA CGU A-3', 5'-GCA UCG AGU GUG UGA ACG A-3', and 5'-CCA GCG ACC CUG ACG ACA A-3') siRNA –SMARTpools were ordered from Dharmacon, and SHARPIN siRNA (5-GCU AGU AAU UAA AGA CAC Ad(TT)-3) and the scramble Allstars negative control siRNA were ordered from QIAGEN. Gene silencing was performed using siRNA oligonucleotides and Lipofectamine RNAiMax reagent (13778150, Thermo Fisher Scientific) according to the manufacturer's protocol. Briefly a mixture in 4:3 ratio (µl RNAiMax: µl siRNA) was prepared in 200 µl optimum and incubated for 20 min before adding to adhered cells grown on a 12-well plate in 400 µl fresh media and cells incubated for 48 h.

Preparation of polyacryl-amide hydrogels. 35 mm glass bottom dishes with 14 mm bottom wells (Cellvis, catalog number D35-14-1-N) were treated with 1 ml Bind silane solution [7.14% Plus One Bind Silane (Sigma, GE17-1330-01), 7.14% acetic acid in 96% ethanol] for 30 min, washed twice with 96% ethanol and left to dry completely. A hydrogel mixture containing 7.5-1% acrylamide solution (Sigma) and 0.06-0.4% bis acryl amide solution (Sigma), diluted in PBS up to a final volume of 500 µl was prepared to obtain hydrogels ranging in stiffness from 0.75-13 kPa. The polymerization of the mixture was initialized by adding 5 µl 10% ammonium persulfate (BioRad) and 1 µl N,N,N,N-Tetramethylethylenediamine (Sigma). The hydrogel solution was quickly vortexed, 11.7 µl was added on top of the glass bottom dish, and a 13 mm glass coverslip carefully placed on top of the drop and the gel was let to polymerize for 1 h RT incubation. After polymerization, the coverslip was carefully removed and the gel incubated with PBS to prevent drying. The stiffness of the hydrogels was confirmed by atomic force microscopy as previously described (37).

Gel surface activation and coating. Gels were incubated for 30 min on slow agitation with 500 µl Sulfo-SANPAH activation solution [0.2 mg/ml Sulfo-SANPAH (Sigma, catalog number 803332), 2 mg/ml N-(3-Dimethylaminopropyl)-N-ethylcarbodiimide hydrochloride (Sigma, catalog number 03450) in 50 mM Hepes] followed by 10 min UV-light activation. After the activation gels were washed three times with PBS and coated with either fibronectin (Merck-Millipore, catalog number 341631) (20 µg/ml) or collagen type I (Merck-Millipore, catalog number 08-115) (20 µg/ml).

Immunofluorescence. Cells were fixed and permeabilized with 0.1% triton in 4% PFA for 8 minutes followed by 10 min fixation with 4% PFA. For antibody staining against integrin α11 samples were fixed with methanol for 10 min -20 C, followed by 10 min 0.1% triton permeabilization in RT. To block unspecific binding of antibodies cells were incubated in 10% horse serum (HRS) for 1 h in RT. Primary and secondary antibodies were diluted in 10% HRS and incubated for 1h in RT. Primary antibodies used: ms anti-vinculin (V9131, Sigma-Aldrich, 1:500), rabbit (rbt) anti-mouse integrin α11 (pro-

vided by Donald Gullberg, 1:200), rat anti-integrin β1, clone MB1.2 (LV1766450, Millipore, 1:100), and mouse (ms) anti-YAP1 (sc-101199, Santa Cruz Biotechnology, 1:100). Secondary antibodies used: Alexa Fluor 488 anti-mouse (A-21202, Thermo Fisher, 1:400), Alexa Fluor 488 anti-rabbit (A-21206, Thermo Fisher, 1:400), Alexa Fluor 647 anti-rat (A-21247, Thermo Fisher 1:400). F-actin was stained with Phalloidin–Atto 647N (65906, Sigma, 1:400), incubated together with secondary antibodies and nuclei with DAPI (D1306, Life Technologies 1:3000) for 10 min RT after secondary antibody incubation. Quantification of the cell area and the number, average size, and average length (Feret diameter ie. the longest distance between any two points along the object boundary, also known as maximum caliper) of adhesions per cell was based on vinculin immunofluorescence labeling.

Confocal imaging. Samples were imaged using 3i (Intelligent Imaging Innovations, 3i Inc) Marianas Spinning disk confocal microscope with a Yokogawa CSU-W1 scanner and Hamamatsu sCMOS Orca Flash 4.0 camera (Hamamatsu Photonics K.K.) using 40x/1.1 water objective), LSM 880 Airyscan laser-scanning confocal microscope (Zeiss) using 20x/0.8 objective, 63x/ 1.4 oil objective or LSM 880 Airyscan LD LCI confocal microscope (Zeiss) using Plan-Apochromat 40x/1.2 water objective and Airyscan detector.

Flow cytometry. MSFs were analysed by flow cytometry as previously described (5). Briefly, cells were detached, placed on ice, fixed with 4% PFA in PBS (10 min RT) and resuspended in PBS. Cell surface integrins were labelled with fluorochrome-conjugated antibodies [Alexa Fluor 488 anti-integrin β1 (Clone: HMβ1-1, Biolegend), APC anti-integrin α1 (Clone: HMα1, Biolegend), or Alexa Fluor 488 anti-integrin α5 (Clone: 5H10-27, Biolegend)] diluted in 100 µL Tyrode's buffer (10 mM HEPES-NaOH at pH 7.5, 137 mM NaCl, 2.68 mM KCl, 1.7 mM MgCl2, 11.9 mM NaHCO3, 5 mM glucose, 0.1% BSA) according to manufacturer's instrctions for 30 min at RT. Alternatively, cells were first labelled with primary antibodies [integrin α11 (AF6498, R&D), or active integrin β1 (clone 9EG7, BD Pharmingen)] followed by secondary antibodies [Alexa Fluor 647 anti-sheep (ab150179, Abcam) or Alexa Fluor 488 anti-rat (Molecular Probes)] both diluted in Tyrode's buffer. After washes, the samples were analysed using BD LSR Fortessa flow cytometer. Live cells were gated from FSC-A/SSC-A dot blot and analysed for geometric mean or median fluorescence intensity. The expression of active integrin β1 was normalized to the total surface expression of integrin β1.

Western blotting. Because of the small hydrogel area (13 mm) on our in-house hydrogels we used the commercial hydrogels Softwell® 6, Easy Coat™ (SW6-EC-0.5, SW6-EC-2 EA, SW6-EC-4 EA and SW6-EC-50 EA, Matrigen) for immunoblotting samples collected from hydrogels. Protein extracts were prepared by lysing the cells with hot TX lysis buffer [50 mM Tris–HCl pH 7.5, 150 mM NaCl, 5% glycerol, 1% SDS, 0.5% Triton X-100, Complete protease inhibitor, PhosSTOP (Roche)]. Samples were sonicated with BioRuptor and protein concentration was measured by Bio-Rad to assure equal protein loading. The protein extract was first separated by loading equal amounts of protein on 4-20% Mini-PROTEAN® TGX™ Gel SDS–PAGE gradient gels (456-1096, Biorad) and then transferred to the nitrocellulose membrane with Trans-Blot Turbo Transfer Pack (170-4159, Biorad). The membrane was blocked for 1 h in RT with 5% milk in Tris Buffered Saline and 0.1% Tween 20 (TBST) solution before antibody incubation. Primary and secondary antibodies were incubated for a minimum of 1 h. Membranes were scanned and results analyzed with the Odyssey infrared system (LICOR Biosciences). Primary antibodies used for western blotting: Rabbit anti-Phospho-Myosin Light Chain 2 (Thr18/Ser19) (3674, Cell Signaling Technology), rabbit anti-Myosin Light Chain 2 (3672, Cell Signaling Technology), mouse anti-glyceraldehyde-3-phosphate dehydrogenase (GAPDH) (5G4-MAb: 6C5, HyTest), rabbit anti-SHARPIN (14626-1-AP, Proteintech) and rabbit anti-Integrin α11 (provided by D. Gullberg). Secondary antibodies used for western blotting: IRDye® 800CW Donkey anti-Mouse IgG, IRDye® 800CW Donkey anti-Rabbit IgG, IRDye® 680LT Donkey anti-Mouse IgG and IRDye® 680LT Donkey anti-Rabbit IgG, diluted 1:10000 in odyssey blocking buffer (LI-COR).

Actin flow. EGFP-LifeAct transfected cells were plated on 2 kPa collagen coated hydrogels and allowed to spread for 45-105 min before image acquisition. Imaging was performed with a Carl Zeiss LSM 880 Airyscan microscope using a 63x/1.4 oil immersion objective and its airyscan detector array. Images were acquired every second for 125 seconds and actin flow was measured based on the slope from kymographs drawn along actin fibers close to the cell periphery at the leading edge.

Traction force microscopy. For traction force microscopy experiments, cells were seeded 4h before performing experiments on polyacrylamide hydrogels of different stiffness prepared as previously described(13). Then, simultaneous images were acquired of single cells (phase contrast) and of fluorescent 200 nm beads embedded in gels. Images were acquired with a Nikon Ti Epifluorescence microscope with a 40x objective (N.A. 0.6). Afterwards, cells were trypsinized, and images of bead positions in the gel in the relaxed state were acquired. By comparing bead positions in the deformed versus relaxed positions, a map of gel displacement caused by cells was measured using a custom particle-imaging-velocimetry software (38). Then, assuming that the displacements were caused by forces exerted by cells on the cell-gel contact area, forces were measured using a previously described Fourier transform algorithm (39, 40). The average forces per unit area of each cell was then measured.

Magnetic tweezers and bead recruitment experiments. Magnetic tweezers experiments were performed as previously described (14, 41, 42). Briefly, 3 µm carboxylated magnetic beads (Invitrogen) were coated with a mixture of bio-

tynilated BSA and either biotynilated fibronectin or collagen I fragment (10:1 ratio). This fragment was pentameric FN7-10 for fibronectin (43) and the GFOGER peptide for collagen I (44). Two hours after seeding cells on glass coverslips, coated magnetic beads were deposited on top of the coverslips and allowed to attach to cells. Then, magnetic beads on the lamellipodia of single cells were pulled with a 1 nN pulsatory force (1 Hz), and the time required to detach beads was measured. To quantify the recruitment of integrin β1, 3 µm carboxylated silica beads (Kisker Biotech) were used and coated as described above. Instead of pulling the beads, cells with silica beads were fixed and stained for integrin β1 (Abcam, 12G10). The average intensity of both beads and surrounding areas was quantified, and the difference between those values was taken as the integrin recruitment measure.

Preparation of micropatterned hydrogels. Crossbow shaped micropatterns were prepared on 13 mm coverslips as previously described (5) and coated with 20 µg/ml collagen I. The micropatterned coverslips were then used in the preparation of 2 kPa PAA hydrogels as described above to create crossbow shaped Collagen I micropatterns on top of the hydrogels.

Mathematical modelling. Modelling was carried out using the molecular clutch model previously described in detail (14). Briefly, the model considers a given number of myosin motors, pulling on an actin bundle. The actin bundle can bind to a set of collagen ligands through molecular clutches that represent adaptor proteins and integrins. In turn, collagen ligands are connected to the substrate through a spring constant representing substrate stiffness. Molecular clutches bind to the collagen ligands with an effective binding rate, and unbind with an unbinding rate that depends on force as a catch bond. The clutches transmit forces to the substrate only when they are bound, and therefore overall force transmission critically depends on binding dynamics. In simulations, all parameters remain constant except the substrate spring constant (which increases with stiffness), and the number of myosin motors pulling on actin, which increases with stiffness following the results in Figure 4D, E. This increase is the same for both wild-type and *Sharpin*^{cpdm} cells. The only parameter that is different in the model between both conditions (wild-type and *Sharpin*^{cpdm}) is the unbinding time. We note that in contrast to our previous work (13, 14, 40), in this case we do not introduce reinforcement in the model, i.e. force-dependent recruitment of additional integrins. This is because focal adhesion size and distribution is largely independent of both stiffness and SHARPIN-deficiency. We also note that for unbinding rate, we took the catch bond force dependence reported in (45) for α5β1 integrins. This dependency is likely to change for collagen-binding integrins, for which unfortunately there are to our knowledge no reported measurements of systematic force-lifetime measurements at the single molecule level. However, whereas specific levels of force depend on this dependence, overall trends with stiffness, and the relative differences if overall unbinding rates are altered (as occurs upon SHARPIN depletion) are maintained regardless of the specific force dependence assumed. See Table 1 for a list of parameters.

Table 1. Parameters for mathematical modelling

Parameter	meaning	Value	Origin
N_{cl}	Number of FN molecules	2000	Adjusted
K_{ont}	True binding rate	0.1×10^{-4} um^2/s	Adjusted, of the order of values reported for αIIBβ3 (46)
n_m	Number of myosin motors	From 1000 at 300 Pa to 18717 at 42129 Pa	Adjusted
F_m	Myosin motor stall force	*2 pN*	(47)
v_u	Unloaded myosin motor velocity	110 nm/s	(14, 48)
d_{int}	Integrin density on the membrane	1600 /μm^2	Set, of the order of reported values (14)
K_{off}	Integrin unbinding rate, scaling factor applied to force curve reported in Kong et al.	0.05 wt 0.4 cpdm	Adjusted, catch bond dependency form (13, 45)
k_c	Clutch spring constant	1 nN/nm	(49)
r_a	Radius of adhesion	1700 nm	Set

Statistical analysis. GraphPad software was used for all statistical analyses. Student's t-test (unpaired, two-tailed) was used when normality could be confirmed by D'Agostino Pearson omnibus normality test. Nonparametric Mann–Whitney U-test was used when two non-normally distributed groups were compared or when normality could not be tested [due to a too small data set (n 8)]. Wilcoxon matched-pairs signed rank test was used if samples with unequal variance were compared. Fisher's exact test was used for the analysis of contingency tables. Data are presented in column graphs with mean ± standard error of mean (SEM) and P-values. Individual data points per condition are shown when n 15, and n-numbers are indicated in figure legends.

ACKNOWLEDGEMENTS

We thank J. Siivonen, and P. Laasola for technical assistance; P. Erusappan for integrin α11 antibody protocols; H. Hamidi for editing of the manuscript; and X. Trepat for thought provoking discussions that inspired this study. Turku Centre for Biotechnology Cell Imaging Core, Turku Center for Disease Modeling and Biocenter Finland are acknowledged for services, instrumentation and expertise. This study has been supported by the Academy of Finland, ERC Consolidator Grant, the Sigrid Juselius Foundation, and the Finnish Cancer Organization. ML has been supported by Turku Doctoral Program of Molecular Medicine, Instrumentarium Science Foundation and The Swedish Cultural Foundation in Finland, and EP by Academy of Finland and Finnish Cultural foundation.

AUTHOR CONTRIBUTIONS

PRC, EP and JI contributed to the conception and design of the study. ML, AEA, MG, JZK and EP designed, conducted and analysed in vitro experiments. AEA and JZK performed traction force microscopy. ML and AEA conducted the magnetic tweezer experiments. CG analysed the TFM data and confirmed gel stiffness with AFM. ML, EP and JI wrote the manuscript, and AEA, PRC, and DG edited the manuscript. DG, PRC, EP and JI supervised the research.

COMPETING FINANCIAL INTERESTS

The authors declare no competing financial interests.

Bibliography

1. Harris AK, Stopak D, Wild P. Fibroblast traction as a mechanism for collagen morphogenesis. Nature. 1981 Mar 19,;290(5803):249-51.

2. Brownfield DG, Venugopalan G, Lo A, Mori H, Tanner K, Fletcher DA, et al. Patterned collagen fibers orient branching mammary epithelium through distinct signaling modules. Curr Biol. 2013 Apr 22,;23(8):703-9.

3. Ingman WV, Wyckoff J, Gouon-Evans V, Condeelis J, Pollard JW. Macrophages promote collagen fibrillogenesis around terminal end buds of the developing mammary gland. Dev Dyn. 2006 Dec;235(12):3222-9.

4. Navab R, Strumpf D, To C, Pasko E, Kim KS, Park CJ, et al. Integrin α11β1 regulates cancer stromal stiffness and promotes tumorigenicity and metastasis in non-small cell lung cancer. Oncogene. 2016 Apr 14,;35(15):1899-908.

5. Peuhu E, Kaukonen R, Lerche M, Saari M, Guzmán C, Rantakari P, et al. SHARPIN regulates collagen architecture and ductal outgrowth in the developing mouse mammary gland. EMBO J. 2017 01 17,;36(2):165-82.

6. Peuhu E, Salomaa SI, De Franceschi N, Potter CS, Sundberg JP, Pouwels J. Integrin beta 1 inhibition alleviates the chronic hyperproliferative dermatitis phenotype of SHARPIN-deficient mice. PLoS ONE. 2017;12(10):e0186628.

7. Rantala JK, Pouwels J, Pellinen T, Veltel S, Laasola P, Mattila E, et al. SHARPIN is an endogenous inhibitor of β1-integrin activation. Nat Cell Biol. 2011 Sep 25,;13(11):1315-24.

8. Pouwels J, De Franceschi N, Rantakari P, Auvinen K, Karikoski M, Mattila E, et al. SHARPIN regulates uropod detachment in migrating lymphocytes. Cell Rep. 2013 Nov 14,;5(3):619-28.

9. Tiger CF, Fougerousse F, Grundström G, Velling T, Gullberg D. alpha11beta1 integrin is a receptor for interstitial collagens involved in cell migration and collagen reorganization on mesenchymal nonmuscle cells. Dev Biol. 2001 Sep 01,;237(1):116-29.

10. Popova SN, Barczyk M, Tiger C, Beertsen W, Zigrino P, Aszodi A, et al. Alpha11 beta1 integrin-dependent regulation of periodontal ligament function in the erupting mouse incisor. Mol Cell Biol. 2007 Jun;27(12):4306-16.

11. Westcott JM, Prechtl AM, Maine EA, Dang TT, Esparza MA, Sun H, et al. An epigenetically distinct breast cancer cell subpopulation promotes collective invasion. J Clin Invest. 2015 May;125(5):1927-43.

12. Elosegui-Artola A, Trepat X, Roca-Cusachs P. Control of Mechanotransduction by Molecular Clutch Dynamics. Trends Cell Biol. 2018 May;28(5):356-67.

13. Elosegui-Artola A, Oria R, Chen Y, Kosmalska A, Pérez-González C, Castro N, et al. Mechanical regulation of a molecular clutch defines force transmission and transduction in response to matrix rigidity. Nat Cell Biol. 2016 05;18(5):540-8.

14. Elosegui-Artola A, Bazellières E, Allen MD, Andreu I, Oria R, Sunyer R, et al. Rigidity sensing and adaptation through regulation of integrin types. Nat Mater. 2014 Jun;13(6):631-7.

15. Erdogan B, Ao M, White LM, Means AL, Brewer BM, Yang L, et al. Cancer-associated fibroblasts promote directional cancer cell migration by aligning fibronectin. J Cell Biol. 2017 11 06,;216(11):3799-816.

16. Glentis A, Oertle P, Mariani P, Chikina A, El Marjou F, Attieh Y, et al. Cancer-associated fibroblasts induce metalloprotease-independent cancer cell invasion of the basement membrane. Nat Commun. 2017 10 13,;8(1):924.

17. Plodinec M, Loparic M, Monnier CA, Obermann EC, Zanetti-Dallenbach R, Oertle P, et al. The nanomechanical signature of breast cancer. Nat Nanotechnol. 2012 Nov;7(11):757-65.

18. Lopez JI, Kang I, You W, McDonald DM, Weaver VM. In situ force mapping of mammary gland transformation. Integr Biol (Camb). 2011 Sep;3(9):910-21.

19. del Rio A, Perez-Jimenez R, Liu R, Roca-Cusachs P, Fernandez JM, Sheetz MP. Stretching single talin rod molecules activates vinculin binding. Science. 2009 Jan 30,;323(5914):638-41.

20. Chen H, Choudhury DM, Craig SW. Coincidence of actin filaments and talin is required to activate vinculin. J Biol Chem. 2006 Dec 29,;281(52):40389-98.

21. Tulla M, Pentikäinen OT, Viitasalo T, Käpylä J, Impola U, Nykvist P, et al. Selective binding of collagen subtypes by integrin alpha 1I, alpha 2I, and alpha 10I domains. J Biol Chem. 2001 Dec 21,;276(51):48206-12.

22. Polte TR, Eichler GS, Wang N, Ingber DE. Extracellular matrix controls myosin light chain phosphorylation and cell contractility through modulation of cell shape and cytoskeletal prestress. Am J Physiol , Cell Physiol. 2004 Mar;286(3):518.

23. Bangasser BL, Rosenfeld SS, Odde DJ. Determinants of maximal force transmission in a motor-clutch model of cell traction in a compliant microenvironment. Biophys J. 2013 Aug 06,;105(3):581-92.

24. Bangasser BL, Shamsan GA, Chan CE, Opoku KN, Tüzel E, Schlichtmann BW, et al. Shifting the optimal stiffness for cell migration. Nat Commun. 2017 05 22,;8:15313.

25. Chan CE, Odde DJ. Traction dynamics of filopodia on compliant substrates. Science. 2008 Dec 12,;322(5908):1687-91.

26. Lehnert K, Ni J, Leung E, Gough SM, Weaver A, Yao WP, et al. Cloning, sequence analysis, and chromosomal localization of the novel human integrin alpha11 subunit (ITGA11). Genomics. 1999 Sep 01,;60(2):179-87.

27. Bansal R, Nakagawa S, Yazdani S, van Baarlen J, Venkatesh A, Koh AP, et al. Integrin alpha 11 in the regulation of the myofibroblast phenotype: implications for fibrotic diseases. Exp Mol Med. 2017 Nov 17,;49(11):e396.

28. Parajuli H, Teh M, Abrahamsen S, Christoffersen I, Neppelberg E, Lybak S, et al. Integrin α11 is overexpressed by tumour stroma of head and neck squamous cell carcinoma and correlates positively with alpha smooth muscle actin expression. J Oral Pathol Med. 2017 Apr;46(4):267-75.

29. Popov C, Radic T, Haasters F, Prall WC, Aszodi A, Gullberg D, et al. Integrins α2β1 and α11β1 regulate the survival of mesenchymal stem cells on collagen I. Cell Death Dis. 2011 Jul 28,;2:e186.

30. Lu Z, Mathew S, Chen J, Hadziselimovic A, Palamuttam R, Hudson BG, et al. Implications of the differing roles of the β1 and β3 transmembrane and cytoplasmic domains for integrin function. Elife. 2016 12 08,;5.

31. Oakes PW, Beckham Y, Stricker J, Gardel ML. Tension is required but not sufficient for focal adhesion maturation without a stress fiber template. J Cell Biol. 2012 Feb 06,;196(3):363-74.

32. Zhu C, Popova SN, Brown ERS, Barsyte-Lovejoy D, Navab R, Shih W, et al. Integrin alpha 11 regulates IGF2 expression in fibroblasts to enhance tumorigenicity of human non-small-cell lung cancer cells. Proc Natl Acad Sci U S A. 2007 Jul 10,;104(28):11754-9.

33. Tamiya H, Kim H, Klymenko O, Kim H, Feng Y, Zhang T, et al. SHARPIN-mediated regulation of protein arginine methyltransferase 5 controls melanoma growth. J Clin Invest. 2018 Jan 02,;128(1):517-30.

34. He L, Ingram A, Rybak AP, Tang D. Shank-interacting protein-like 1 promotes tumorigenesis via PTEN inhibition in human tumor cells. J Clin Invest. 2010 Jun;120(6):2094-108.

35. Seymour RE, Hasham MG, Cox GA, Shultz LD, Hogenesch H, Roopenian DC, et al. Spontaneous mutations in the mouse Sharpin gene result in multiorgan inflammation, immune system dysregulation and dermatitis. Genes Immun. 2007 Jul;8(5):416-21.

36. HogenEsch H, Gijbels MJ, Offerman E, van Hooft J, van Bekkum DW, Zurcher C. A spontaneous mutation characterized by chronic proliferative dermatitis in C57BL mice. Am J Pathol. 1993 Sep;143(3):972-82.

37. Närvä E, Stubb A, Guzmán C, Blomqvist M, Balboa D, Lerche M, et al. A Strong Contractile Actin Fence and Large Adhesions Direct Human Pluripotent Colony Morphology and Adhesion. Stem Cell Reports. 2017 07 11,;9(1):67-76.

38. Bazellières E, Conte V, Elosegui-Artola A, Serra-Picamal X, Bintanel-Morcillo M, Roca-Cusachs P, et al. Control of cell-cell forces and collective cell dynamics by the intercellular adhesome. Nat Cell Biol. 2015 Apr;17(4):409-20.

39. Butler JP, Tolić-Nørrelykke IM, Fabry B, Fredberg JJ. Traction fields, moments, and strain energy that cells exert on their surroundings. Am J Physiol , Cell Physiol. 2002 Mar;282(3):595.

40. Oria R, Wiegand T, Escribano J, Elosegui-Artola A, Uriarte JJ, Moreno-Pulido C, et al. Force loading explains spatial sensing of ligands by cells. Nature. 2017 12 14,;552(7684):219-24.

41. 41. Roca-Cusachs P, Gauthier NC, Del Rio A, Sheetz MP. Clustering of alpha(5)beta(1) integrins determines adhesion strength whereas alpha(v)beta(3) and talin enable mechanotransduction. Proc Natl Acad Sci U S A. 2009 Sep 22,;106(38):16245-50.

42. González-Tarragó V, Elosegui-Artola A, Bazellières E, Oria R, Pérez-González C, Roca-Cusachs P. Binding of ZO-1 to α5β1 integrins regulates the mechanical properties of α5β1-fibronectin links. Mol Biol Cell. 2017 Jul 07,;28(14):1847-52.

43. Coussen F, Choquet D, Sheetz MP, Erickson HP. Trimers of the fibronectin cell adhesion domain localize to actin filament bundles and undergo rearward translocation. J Cell Sci. 2002 Jun 15,;115(Pt 12):2581-90.

44. Emsley J, Knight CG, Farndale RW, Barnes MJ, Liddington RC. Structural basis of collagen recognition by integrin alpha2beta1. Cell. 2000 Mar 31,;101(1):47-56.

45. Kong F, García AJ, Mould AP, Humphries MJ, Zhu C. Demonstration of catch bonds between an integrin and its ligand. J Cell Biol. 2009 Jun 29,;185(7):1275-84.

46. Litvinov RI, Mekler A, Shuman H, Bennett JS, Barsegov V, Weisel JW. Resolving two-dimensional kinetics of the integrin αIIbβ3-fibrinogen interactions using binding-unbinding correlation spectroscopy. J Biol Chem. 2012 Oct 12,;287(42):35275-85.

47. Molloy JE, Burns JE, Kendrick-Jones J, Tregear RT, White DC. Movement and force produced by a single myosin head. Nature. 1995 Nov 09,;378(6553):209-12.

48. Chan CE, Odde DJ. Traction dynamics of filopodia on compliant substrates. Science. 2008 Dec 12,;322(5908):1687-91.

49. Roca-Cusachs P, Iskratsch T, Sheetz MP. Finding the weakest link: exploring integrin-mediated mechanical molecular pathways. J Cell Sci. 2012 Jul 01,;125(Pt 13):3025-38.